Iranian Journal of Geophysics, Vol 20 No 6, 2027, Page 75 – 90 (Research Article)
DOI: 10.30499/ijg.525910.1700

Coupled hydrogeophysical finite-element modeling of subsurface flow and ion diffusion for porphyry copper exploration

Amir Yazdanpanah[1] and Maysam Abedi [2*]

[1] *M.Sc., School of Mining Engineering, College of Engineering, University of Tehran, Tehran, Iran*
[2] *Associate Professor., School of Mining Engineering, College of Engineering, University of Tehran, Tehran, Iran*

(Received: 24 May 2025, Accepted: 29 September 2025)

Summary

Porphyry copper deposits play a critical role in global metal supply, emphasizing the need for non-invasive exploratory geophysical techniques to identify mineralized zones at depth. This study employs coupled hydro-geophysical finite-element modeling within the a 2D framework to simulate groundwater flow, ion diffusion, and time-lapse electrical resistivity in a plausible geological domain representative of near-surface porphyry copper systems. The model considers fluid flow through layered geological units and a mineralized zone, while tracking ion transport to mimic copper leaching. Meanwhile, real-time electrical resistivity tomography (ERT) captures electrical resistivity variations induced by ion concentrations. Additionally, the ERT data are then inverted using the Conjugate Gradient Least Squares (CGLS) algorithm, allowing the reconstruction of four 2D electrical resistivity models that illustrate the evolution of the mineralized zone over time. The results highlight distinct flow and concentration patterns, with the inverted electrical resistivity models aligning with the velocity gradients from the forward simulations, improving the detection of the target zone. This integrated approach combines hydrological and geophysical perspectives, providing a scalable framework to optimize drilling strategies while minimizing environmental impact. This innovative approach serves as a non-invasive tool for the exploration of porphyry copper deposits, offering a highly effective methodoslogy for detecting mineral resources beneath the earth's surface. The precision and reliability of this exploration tool not only enhance the efficiency of mineral deposit identification but also contribute to more sustainable mining practices.

Keywords: Porphyry copper, hydro-geophysical modeling, ion diffusion, time-lapse electrical resistivity (ERT)

[*]Corresponding author: maysamabedi@ut.ac.ir

1 Introduction

Porphyry copper deposits are cornerstone resources in the global mining industry, supplying over 60% of the world's copper, a critical metal for renewable energy systems, electric vehicles, and modern infrastructure. These deposits, formed in complex geological settings with heterogeneous host rocks and mineralized zones, present significant exploration challenges due to their depth and structural variability (Berger et al., 2008). Traditional exploration methods, such as extensive drilling, are resource-intensive, environmentally disruptive, and often inefficient in pinpointing subsurface targets. As the demand for copper escalates alongside global sustainability goals, non-invasive exploration techniques have become essential to delineate mineralized zones with precision while minimizing ecological footprints (Nwankwoala & Udom, 2009). Hydro-geophysics, an interdisciplinary field that integrates hydrological and geophysical methodologies, offers a promising solution by enabling detailed characterization of subsurface properties and dynamic processes, such as fluid flow and solute transport (Binley, 2015; Moysey, 2007).

The emergence of hydro-geophysics over the past few decades has transformed subsurface investigation, driven by advancements in geophysical imaging and computational modeling (Binley et al., 2015). Unlike traditional hydrological methods that rely on sparse borehole data, hydro-geophysical approaches leverage large geophysical datasets to infer hydraulic properties, fluid dynamics, and biogeochemical interactions across multiple scales (Moysey, 2007). A foundational principle of hydro-geophysics is the relationship between electrical and hydraulic properties, where electrical resistivity correlates with hydraulic conductivity, porosity, and fluid saturation (Lesmes & Friedman, 2005; Mazáč et al., 1985). These correlations enable techniques like electrical resistivity tomography (ERT) to monitor subsurface changes, such as those induced by fluid flow or ion transport, making ERT particularly valuable for detecting mineralized zones in porphyry copper systems (Johnson et al., 2010). For example, resistivity anomalies can indicate the presence of conductive fluids or mineralized alteration zones, guiding exploration efforts with greater accuracy.

Historically, hydro-geophysical studies relied on uncoupled approaches, where geophysical data were inverted independently to estimate properties like electrical conductivity, which were then translated into hydrological parameters using petrophysical relationships (Hinnell et al., 2010). However, uncoupled methods often introduce errors due to mismatched assumptions and data inconsistencies. Recent advancements in coupled hydro-geophysical inversion have addressed these limitations by directly integrating hydrological and geophysical models during parameter estimation, preserving process interactions and reducing uncertainty (González-Quirós & Comte, 2021; Hinnell et al., 2010). In this context, inversion plays a critical role in ERT by reconstructing subsurface resistivity distributions from apparent resistivity measurements, allowing the identification of mineralized zones through iterative optimization and regularization to handle the ill-posed nature of the problem. Coupled inversion leverages finite-element modeling to simulate complex subsurface processes, such as groundwater flow and solute transport, while simultaneously incorporating geophysical data to

constrain parameter estimates, enhancing the accuracy of mineral detection. The advent of parallel computing has further enhanced these capabilities, enabling the processing of large ERT datasets for real-time monitoring of subsurface dynamics, as demonstrated in applications ranging from aquifer characterization to contaminated site remediation (Johnson et al., 2010).

Despite these advancements, hydro-geophysical modeling faces significant challenges in achieving geological realism and predictive accuracy. Geophysical inversion tools often produce smooth property distributions that conflict with the heterogeneous, discontinuous structures typical of porphyry copper deposits (Linde, 2014; Linde et al., 2015). This mismatch can lead to biased parameter estimates, particularly for hydraulic conductivity or recharge rates, which in turn affect model predictions. For instance, studies have shown that inaccurate recharge parameterization can result in poor predictions of groundwater flow paths and solute transport, critical for mineral exploration (Christensen et al., 2016). Additionally, the integration of geophysical data into hydrological models requires robust calibration strategies to account for uncertainties in petrophysical relationships and geophysical measurements (González-Quirós & Comte, 2021). Linde (2014) emphasized the need for falsification strategies, such as using geophysical data to test competing conceptual models, to ensure models reflect true subsurface conditions.

The complexity of porphyry copper systems, characterized by layered geological units and mineralized alteration zones, underscores the need for integrated modeling approaches that capture both hydrological and geophysical signatures. Current literature highlights a gap in applying coupled hydro-geophysical models specifically to mineral exploration, where fluid flow and ion transport play critical roles in shaping geophysical anomalies (Binley, 2015; Nwankwoala & Udom, 2009). While hydrogeophysics has been extensively applied to aquifer studies and environmental monitoring, its potential in detecting mineralized zones in porphyry systems remains underexplored, particularly using finite-element frameworks that simulate dynamic processes like copper leaching.

This study addresses these gaps by developing a coupled hydro-geophysical finite-element model to simulate subsurface flow, ion diffusion, and time-lapse ERT in a 2D geological framework representative of near-surface porphyry copper deposits. Implemented using the pyGIMLi framework, the model integrates groundwater flow through layered geological units with a mineralized zone, tracking ion transport to mimic copper leaching processes. Time-lapse ERT, supported by advanced inversion techniques, captures resistivity changes driven by ion concentration variations, revealing the mineralized zone's geophysical signature. Building on established hydro-geophysical principles, the study advances the application of finite-element modeling and inversion to complex mineral exploration scenarios, contributing to the growing body of research on integrated subsurface characterization.

In this study, simulation is employed for a synthetic layered model through unstructured meshing, conducted by utilizing pyGIMLi library, version 1.4.3. The operating system used for the forward and inverse modeling is a laptop with 16GB RAM and a 12th Gen Intel® Core™ i7 1255U CPU.

2 Methodology

This study develops a coupled hydro-geophysical finite-element model to simulate subsurface flow, ion diffusion, and time-lapse ERT in a 2D geological framework representative of shallow porphyry copper deposits. Implemented using the pyGIMLi framework, the model integrates groundwater flow through layered geological units (aquifer, host rock, basement) with a mineralized zone, tracking ion transport to mimic copper leaching and detecting resistivity anomalies via ERT. The methodology employs established governing equations, finite-element methods (FEM), and petrophysical relationships, ensuring scientific validity through rigorous numerical modeling (Rücker et al., 2017).

2.1 Forward Modeling

The simulation process in this study seeks to model the hydro-geophysical dynamics of a porphyry copper deposit to facilitate non-invasive exploration of subsurface mineralized zones, drawing on conceptual insights from fractured media behavior.

Fluid flow in a porous medium is modeled using Darcy's Law for slow, non-viscous, and non-frictional hydraulic movement, as expressed below:

$$K^{-1}\mathrm{v} + \nabla p = 0 \quad (1)$$

$$\nabla \cdot \mathrm{v} = 0 \quad (2)$$

Where v is the Darcy velocity (m/s), K is the hydraulic conductivity (m/s), and p is the hydraulic head (m). Combining these, the governing equation for steady-state flow is:

$$\nabla \cdot (K \nabla p) = 0 \text{ on} \Omega \quad (3)$$

This equation is solved over the 2D domain Ω with Dirichlet boundary conditions, which fix hydraulic head values at the domain's lateral boundaries to simulate a regional hydraulic gradient typical of porphyry systems. The hydraulic velocity is then calculated as:

$$\mathrm{v} = -\nabla p \quad (4)$$

This velocity field drives ion transport in the subsequent advection-diffusion simulation.

Copper ion transport is modeled using the advection-diffusion equation, as shown below:

$$\frac{\partial c}{\partial t} = \nabla \cdot (D \nabla c) - \nabla \cdot (\mathrm{v} c) + S \quad (5)$$

Where $c(r,t)$ is the ion concentration (kg/m³), D is the dispersion tensor (m²/s), v is the Darcy velocity (m/s), and S is a source term (kg/m³·s). The first term, $\nabla \cdot (D \nabla c)$, represents diffusion and dispersion, while the second, $-\nabla \cdot (vc)$, accounts for advection. The dispersion tensor D incorporates longitudinal and transverse dispersivity, which govern the spread of ions due to mechanical mixing and molecular diffusion in heterogeneous media. Dispersivity is parameterized to reflect typical values for fractured and porous rocks, ensuring realistic copper leaching patterns (Hinnell et al., 2010). The source term (S) is modeled as a continuous point source located at coordinates [-22.8, -5.4] m, near the mineralized zone, with a strength of 1 g/l.s, normalized by cell size, and is active for 250 days to simulate copper ion injection, mimicking a leaching process.

The advection-diffusion equation (Equation 5) is solved using the finite volume method in pyGIMLi with the Patankar-Spalart scheme, which employs the Crank-Nicolson method for the diffusion term to ensure numerical stability and second-order accuracy in time. The Crank-Nicolson scheme averages the diffusion term over the current and next time steps, as shown in its simplified form for a 1D diffusion equation (Østerby, 2002):

$$\frac{u_i^{n+1} - u_i n}{\Delta t} = \frac{D}{2} \frac{\partial^2 u}{(\partial x^2)(u_{n+1} + u_n)} \quad (6)$$

In this equation, $u_i n$ represents the ion concentration in kilograms per cubic meter at a specific spatial grid point *i* and time step *n*, while u_i^{n+1} is the concentration at the same grid point at the next time step n+1. The term Δt is the time step in seconds, defining the temporal interval between n and n+1, set to 432 seconds in this study with 50,000 steps over 250 days. The parameter *D* denotes the diffusion coefficient in square meters per second, scaled by dispersivity to account for ion spreading in the porous medium.

The numerical stability of the advection-diffusion simulation is influenced by the Courant-Friedrichs-Lewy (CFL) number (Warburton & Hagstrom, 2008), a dimensionless parameter that governs the relationship between the time step, spatial discretization, and velocity in time-dependent simulations. The CFL number is defined as:

$$\mathrm{CFL} = \frac{v_{\max} \Delta t}{\Delta x} \quad (7)$$

Where v_{max} the maximum Darcy velocity (m/s), Δt is the time step (s), and Δx is the minimum grid cell size.

To ensure numerical stability in the advection-diffusion simulation, the model design was refined by adjusting hydraulic conductivity (K) values to a maximum of 2.12×10^{-5} m/s, and enhancing mesh resolution to a minimum cell size of approximately 0.146 m, resulting in a CFL number of approximately 0.063, well below the threshold of 1.

Changes in electrical resistivity driven by ion concentration are modeled using Archie's Law, a petrophysical relationship linking hydrological and geophysical properties (Lovell & Pezard, 1990):

$$\rho = \rho_w \phi^{-m} \quad (8)$$

Where ρ is the bulk electrical resistivity (Ω·m), ρ_w is the pore fluid resistivity (Ω·m, inversely proportional to ion concentration), ϕ is porosity, and m is the cementation exponent. The ERT forward model solves the Poisson equation for the electrical potential *Φ(V)*:

$$\nabla \cdot (\sigma \nabla \Phi) = 0 \quad (9)$$

Where $\sigma = \frac{1}{\rho}$ is the electrical conductivity (S/m). This equation is derived from hydro-geophysical modeling by relating σ to ion concentration via Archie's Law, enabling ERT to detect electrical resistivity anomalies caused by copper ion migration (Lesmes & Friedman, 2005; Telford et al., 1990).

The governing equations are solved using the finite-element method (FEM) within pyGIMLi, a robust platform for hydro-geophysical modeling. FEM discretizes the 2D domain into a mesh of triangular elements, numerically approximating the hydraulic head, ion concentration, and electrical potential fields. Mesh refinement is applied around the mineralized zone to capture sharp property contrasts. The FEM solver first computes the hydraulic head distribution, derives the velocity field, and then simulates ion transport. The resulting concentrations inform the apparent resistivity distribution via Archie's Law, which is used in the ERT forward model. FEM's flexibility ensures accurate representation of heterogeneous geology and complex boundary conditions (González-Quirós & Comte, 2021).

The 2D subsurface domain is discretized through Delaunay triangulation (DT), with each triangular cell assigned uniform properties. This unstructured mesh configuration facilitates finite element modeling for time-lapse ERT simulations, effectively capturing the intricate

geological structures in the model. To assess the mesh quality, the η metric is employed, which quantifies the relationship between a triangle's area a and the sum of its squared edge lengths ($l_1^2 + l_2^2 + l_3^2$). A normalization constant of $4\sqrt{3}$ is applied, ensuring that an equilateral triangle yields η=1 (Field, 2000). The metric is defined as:

$$\eta = \frac{4\sqrt{3}a}{l_1^2 + l_2^2 + l_3^2} \quad (10)$$

Time-lapse ERT simulates surface-based dipole-dipole measurements, capturing resistivity changes over multiple time steps. The Poisson equation is solved using FEM to compute apparent resistivities, followed by inversion to reconstruct the subsurface resistivity distribution. This identifies anomalies associated with the mineralized zone (Johnson et al., 2010). The coupled approach ensures hydrological and geophysical models are consistent, reducing inversion errors compared to uncoupled methods (Hinnell et al., 2010).

2.2 Inverse Modeling

Inverse modeling in ERT aims to deduce subsurface properties from measured geophysical data, contrasting with forward modeling by addressing inherently non-linear and ill-posed problems prone to geological uncertainties and measurement errors. In this study, ERT inversion converts apparent resistivity data, obtained at various subsurface points, into true resistivity distributions, enabling the identification of geological layers such as the aquifer, host rock, basement, and mineralized zone. The non-unique nature of these solutions requires iterative optimization and constraints to produce reliable outcomes. Here, the inversion is executed using the pyGIMLi framework, employing the conjugate gradient least squares (CGLS) method to iteratively minimize the difference between observed and predicted data, stabilizing the ill-posed problem through regularization techniques. Finite element methods solve the underlying equations numerically, leveraging advancements in computational power to enhance inversion accuracy. Subsurface properties, specifically electrical resistivity, are discretized via unstructured meshes, allowing detailed modeling of the complex geological features within the 2D domain. Developments in inversion strategies continue to improve optimization approaches, addressing data inconsistencies and bolstering the dependability of subsurface models in intricate geological settings (Akingboye & Ogunyele, 2019).

To stabilize the inversion, a regularization approach is applied, with the objective function defined as:

$$\phi = \left\| W_d\left(d_i - f_i(m)\right)\right\|_2^2 + \lambda \| W_m m \|_2^2 \quad (11)$$

Here, d_i denotes the observed apparent resistivity data, $f_i(m)$ represents the forward-modeled data based on the model parameters m, W_d is the data weighting matrix, m encompasses the model parameters such as resistivity, W_m is the model weighting matrix enforcing smoothness, and lambda is the regularization parameter balancing data fit and model complexity.

The inversion iteratively updates the subsurface model by adjusting the current model m_k with an update vector delta m, resulting in the updated model m_{k+1}. At each iteration, the Jacobian matrix *J*, which quantifies the sensitivity of the modeled data to changes in model parameters, is computed (Yazdanpanah & Abedi, 2024). These are expressed as:

$$m_{k+1} = m_k + \Delta m \quad (12)$$

$$J_{i,j} = \partial F_i / \partial m_j \quad (13)$$

In the CGLS method, the update Δm is determined by solving the normal equations (Lu et al., 2024):

$$J_T W_d W_d{}^T J_{\Delta \mathrm{m}} = J_T W_d W_d{}^T (d - f(m_k)) \quad (14)$$

This approach optimizes the model for the 2D geological framework, aligning with the study's focus on porphyry copper systems (Portniaguine & Zhdanov, 1999).

The accuracy of the inversion is assessed using the χ_N^2 parameter, which measures the discrepancy between observed and modeled ERT data. The observed data d_i (apparent resistivity ρ_a) are compared to the modeled data $f_i(m)$, weighted by data uncertainties ϵ_i, with $i = 1, \ldots, N$:

$$\chi^2 = \sum_{i=1}^{N} \left(\frac{d_i - f_i(m)}{\epsilon_i} \right)^2 \quad (15)$$

Ideally, χ^2 should approach N (the number of data points) when the model fits the data within the noise level, and χ_N^2 should be close to 1, indicating an optimal balance between data fit and model complexity. Values of χ_N^2 near 1 enhance confidence in the detection of the mineralized zone, while deviations suggest potential issues with model fit or uncertainty estimates.

3 Hydro-geophysical simulation

The hydro-geophysical modeling of this study begins with the definition of a 2D geological domain representative of a porphyry copper deposit, designed to simulate subsurface flow and ion transport for non-invasive exploration. Table. 1 shows the values of hydraulic conductivity in different rock types. The domain spans a cross-sectional area with a surface layer at z = 0 m and extends to a depth of −19.2 m, divided into three primary geological layers. The aquifer is modeled as a high-porosity sandstone formation, characterized by significant water-bearing capacity, while the host rock is represented by a moderately fractured altered granodiorite layer, typical of porphyry systems hosting mineralized zones. The basement consists of impermeable granite, limiting vertical flow. Embedded within the host rock, a mineralized zone, composed of sulfide-rich fractured rock, reflecting the porphyry copper deposit's geological signature. Hydraulic conductivity values are assigned to reflect these material properties.

Table 1. Hydraulic conductivity values in typical rock types (Notario del Pino & Díaz, 1998).

Material	Hydraulic Conductivity (m/s)
Gravel	10^{-3} – 1
Sand	10^{-5} – 10^{-2}
Silt	10^{-8} – 10^{-5}
Clay	10^{-13} – 10^{-9}
Sandstone	10^{-10} – 10^{-5}
Limestone	10^{-10} – 10^{-7}
Shale	10^{-13} – 10^{-9}
Crystaline Rocks	10^{-13} – 10^{-10}

This geometry is constructed using the pyGIMLi framework, where an unstructured mesh is created with specified layer boundaries, and a rectangular block is added to represent the mineralized zone (Table. 2). Fig. 1a depicts a plausible subsurface medium while Fig. 1b shows a 2D hydro-geophysical model. Also, Fig. 1c presents the initial resistivity model, illustrating the baseline electrical properties of the geological units before ion migration.

The model domain, with a depth of 19.2 m and width of 48 m, is intentionally designed to represent near-surface porphyry copper systems, where significant erosion has brought mineralized zones closer to the surface. In many regions, porphyry and epithermal copper deposits are characterized by shallow occurrences due to extensive erosional processes, making such scales relevant for exploration. This configuration is thus suitable for studying near-surface alteration zones and ion transport dynamics, aligning with the study's focus on non-invasive hydro-geophysical techniques for detecting accessible mineralized targets.

Table 2. Geological and Hydrological Properties of the Model.

Geological Unit	Depth	Material	Hydraulic conductivity	Electrical Resistivity (Ω.m)
Layer 1: Aquifer	0 – 2.4 (2.4 m)	Sandstone	1×10^{-5}	50
Laye 2: Host Rock	2.4 - 9.6 (7.2 m)	Altered Granodiorite	1×10^{-6}	500
Layer 3: Basement	9.6 - 19.2 (9.6 m)	Granite	1×10^{-8}	2000
Mineralized Zone	4.2 – 7.2 (3 m)	sulfide-rich fractured rock	5×10^{-6}	10

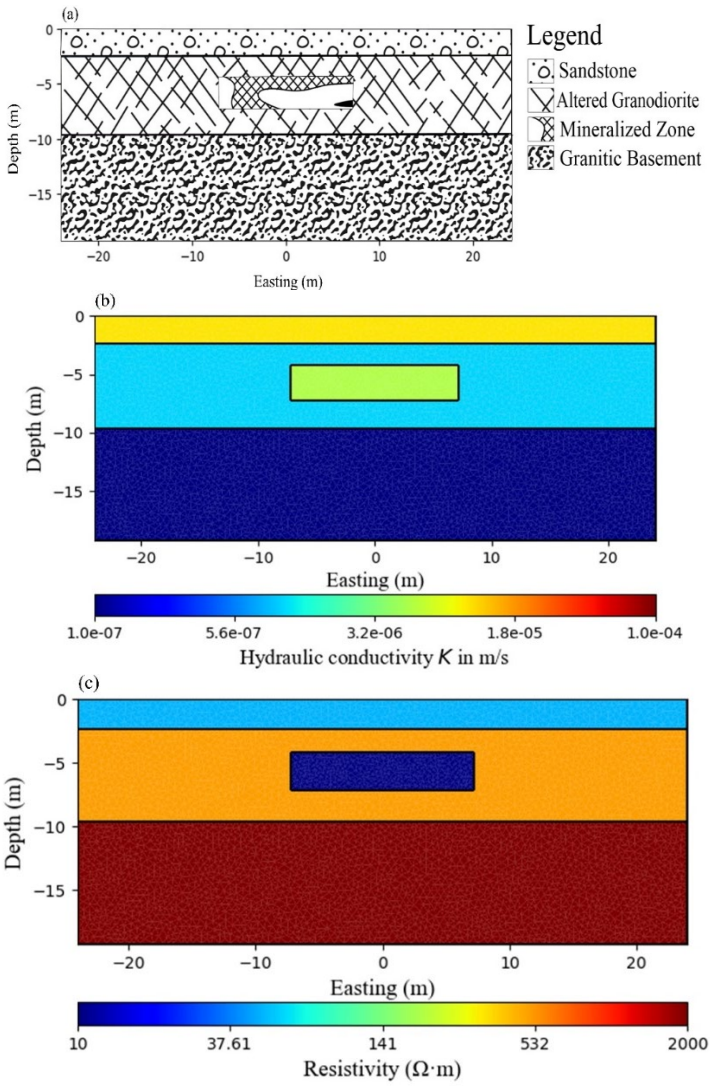

Figure 1. Geological and hydraulic conductivity profiles of the 2D model: (a) A plausible representation of the aquifer, host rock, basement, and mineralized zone with; (b) hydraulic conductivity distribution (in m/s), highlighting permeability variations across the layers on a logarithmic scale.

The mesh is generated using the pyGIMLi meshing module, discretizing the 2D domain into a finite-element structure that captures the layered geology and mineralized zone. The geometry features a symmetrical cross-section from [−24, 0] m to [24, −19.2] m, with layer boundaries at −2.4 m and −9.6 m, and includes a distinct mineralized block from −7.2 m to 7.2 m horizontally and −4.2 m to −7.2 m vertically. Refinement around the mineralized zone ensures accurate representation of its hydraulic properties, while a quality-controlled mesh supports the assignment of hydraulic conductivity values, mapped to each region (aquifer, host rock, basement, and mineralized zone) to reflect their geological characteristics. Fig. 2a shows the mesh quality of the provided model while Fig. 2b illustrates the quality distribution in the same model.

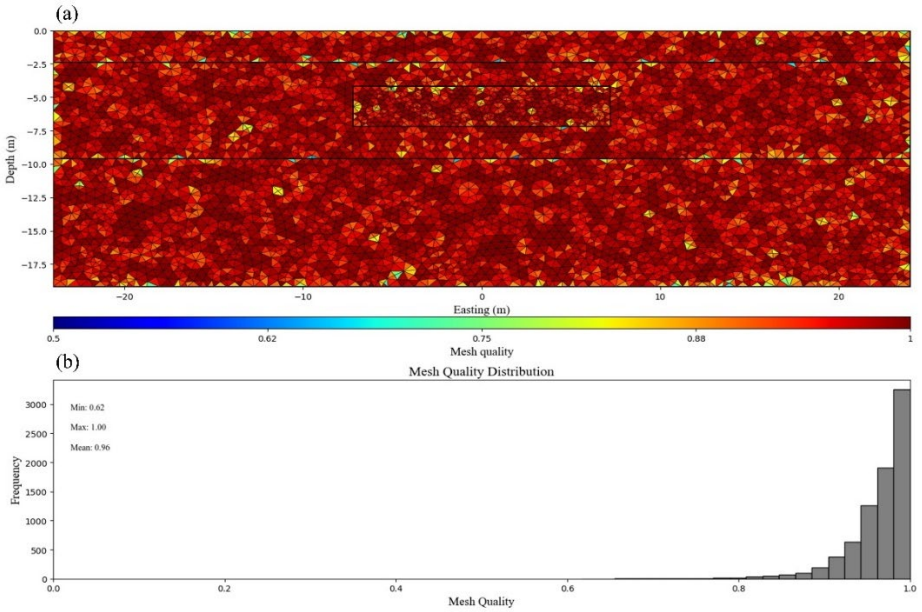

Figure 2. (a) Forward mesh quality; (b) Mesh quality distribution.

4 Results and discussion

The hydro-geophysical modeling yields key insights into the subsurface dynamics of a porphyry copper deposit, starting with the simulation of hydraulic potential and velocity. Dirichlet boundary conditions establish a hydraulic gradient across the 2D domain, with higher potential on the left and lower on the right, driving groundwater flow. The resulting velocity field, visualized in Fig. 3, highlights flow patterns, with enhanced movement through the high-permeability aquifer and mineralized zone, reflecting their geological properties. This velocity distribution serves as a critical input for subsequent ion transport, demonstrating how hydraulic conductivity variations influence flow dynamics in the system.

Ion concentration evolution, depicted in Fig. 4 with eight subfigures (Fig. 4a to 4h), illustrates the transport of copper ions over a 250-day period. The simulation tracks a continuous injection phase over 250 days, with eight evenly spaced snapshots capturing the ion concentration evolution approximately every 36 days. Each subfigure represents a time step, showing the spread of ions from the injection point through advection and diffusion, modulated by the velocity field and

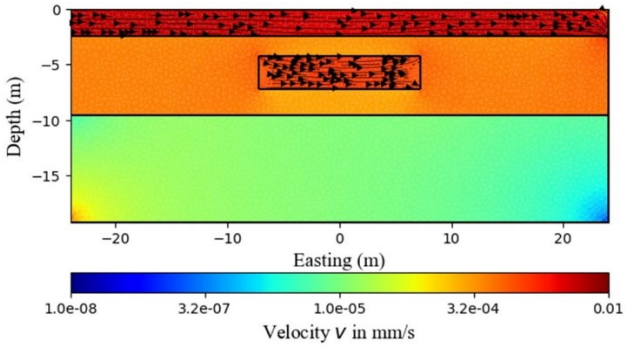

Figure 3. Velocity field distribution in the 2D geological model, illustrating groundwater flow patterns (in mm/s) influenced by hydraulic conductivity variations across the aquifer, host rock, basement, and mineralized zone.

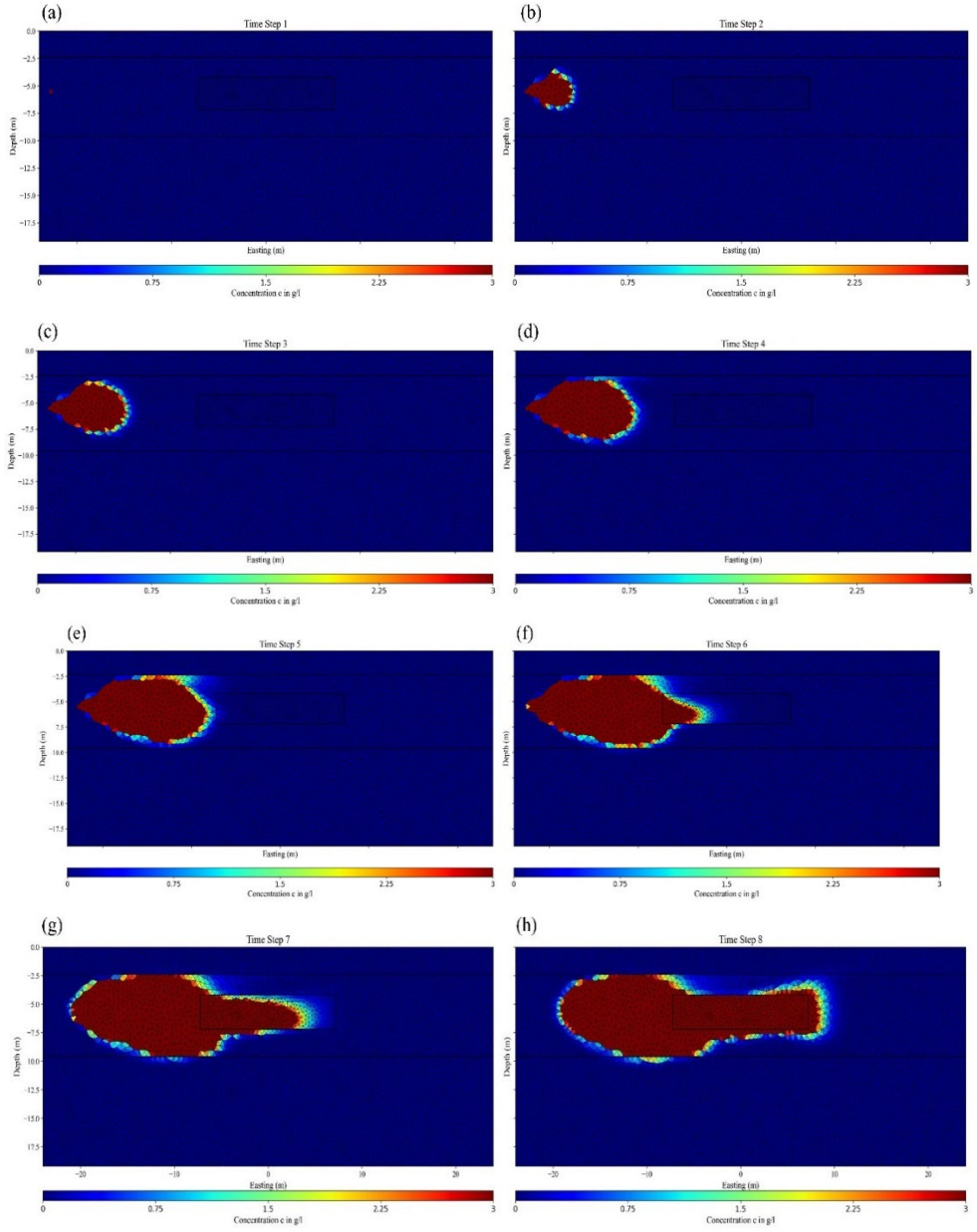

Figure 4. Ion concentration evolution over 250 days in the 2D model, showing eight snapshots (a–h) of copper ion distribution (in g/l) from injection to dispersion, highlighting leaching dynamics in the mineralized zone.

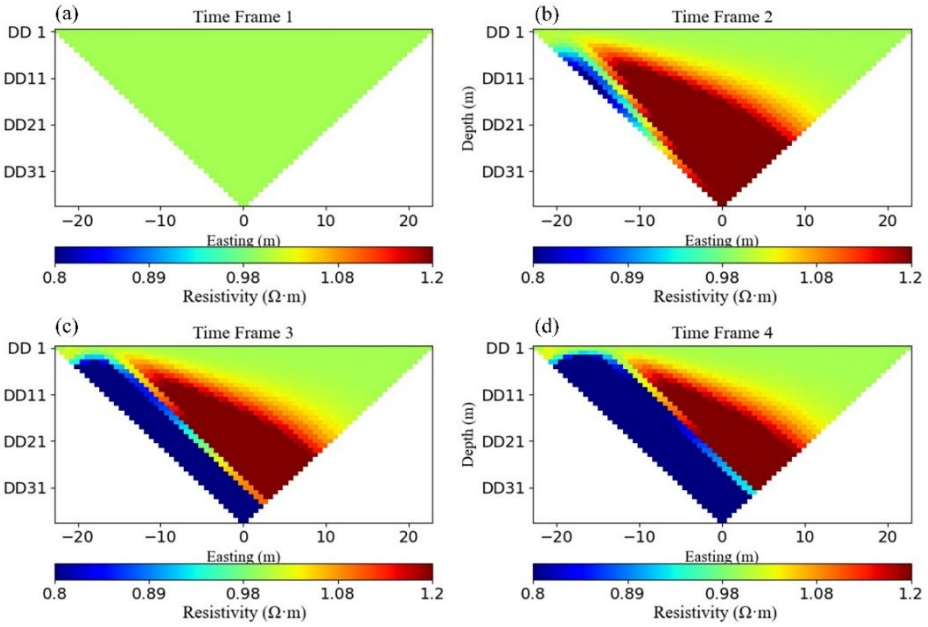

Figure 5. Observed apparent resistivity ratios for four time frames (a-d) before inversion.

dispersivity. The concentration increases initially near the mineralized zone, then disperses outward, with Fig. 4a marking the start and Fig. 4h the end, providing a comprehensive view of leaching dynamics. This slow and temporal sequence underscores the effectiveness of the coupled model in tracking ion migration, offering insights into mineralized zone detection.

ERT results, presented in Fig. 5 with four subfigures (Fig. 5a to 5d), reveal observed apparent resistivity ratios over selected time frames, reflecting changes due to ion concentration. The four plots correspond to four distinct time points within the 250-day period, chosen to highlight significant shifts in subsurface resistivity as ions alter the fluid conductivity. Each subfigure shows the ratio of apparent resistivity to the initial state, with values indicating anomalies linked to the mineralized zone. Fig. 5a represents the earliest change, while Fig. 5d captures the latest, illustrating how ERT detects temporal resistivity variations. This analysis validates the model's ability to integrate hydrological and geophysical data, enhancing the identification of copper-rich zones with minimal surface disturbance.

The inversion of time-lapse ERT data was performed using the pyGIMLi framework, employing the CGLS algorithm to reconstruct subsurface electrical resistivity distributions. This iterative method minimizes the misfit between observed apparent resistivity ratios (Figs. 5a–5d) and predicted responses (Fig. 6), regularized with a vertical weighting factor to enhance depth resolution. Each of the four time frames underwent a separate inversion run with a regularization parameter which targets smoothness, ensuring stability while preserving geological features. The CGLS algorithm efficiently converged, producing reliable resistivity models, as visualized in Figs. 8a–8d.

Smoothness-constrained Tikhonov regularization was employed for the inversion of ERT data, promoting spatially smooth resistivity distributions while balancing data fit and model complexity. A regularization parameter of 5 was applied, with a vertical-to-

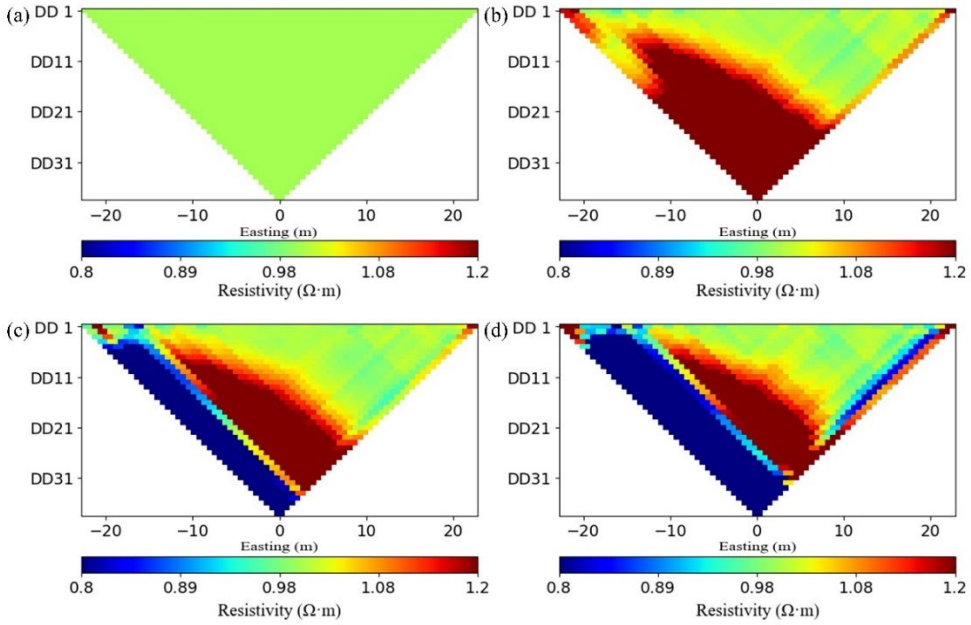

Figure 6. Predicted apparent resistivity ratios for four time frames (a-d) after inversion.

horizontal smoothness weighting of 0.1 to account for layered geological structures. Resistivity values were constrained between 1 and 5000 Ω·m to ensure physical realism, and the inversion mesh was limited to a maximum cell size of 1 m² with a maximum depth of 25 m to maintain resolution near the mineralized zone. These settings ensured stable and geologically plausible inverted resistivity models across the four time frames.

The misfit between observed and predicted apparent resistivities, presented in Figs. 7a–7d, provides a quantitative measure of inversion accuracy across the four time frames. These pseudosection plots highlight spatial variations in relative misfit. The inverted electrical

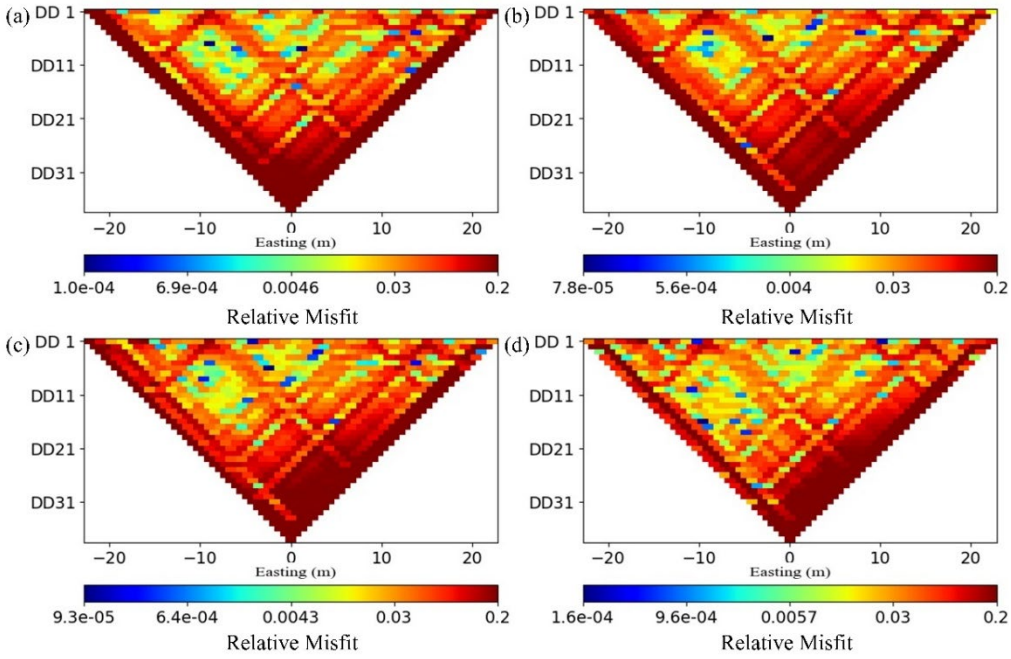

Figure 7. Misfit plot of apparent resistivity ratios (a-d).

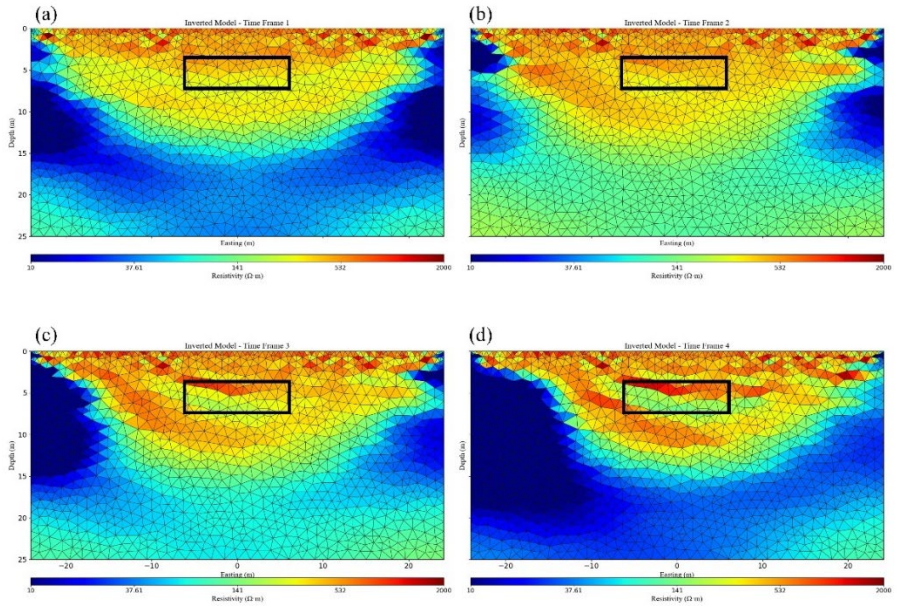

Figure 8. Inverted 2D electrical resistivity models from time-lapse ERT for four time frames (a–d), corresponding to the ERT ratio datasets, highlighting the mineralized zone's evolution (in Ω·m).

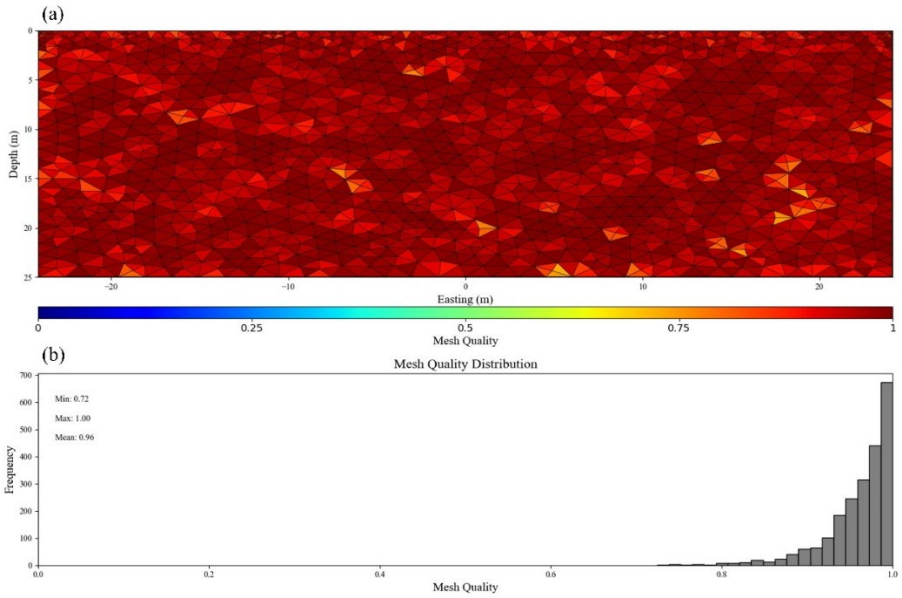

Figure 9. (a) Inversion mesh quality; (b) Mesh quality distribution.

resistivity models (Figs. 8a–8d) demonstrate strong compatibility with the forward modeling results, particularly the velocity gradient derived from hydraulic potential simulations. The predicted apparent resistivity ratios (Fig. 6) further validate the inversion by showing consistency with the observed data. The low-resistivity anomalies in the mineralized zone align with enhanced flow patterns observed in Fig. 3, reflecting the influence of ion migration on electrical properties. The quality of the inversion mesh, distinct from the forward mesh in refinement and parameterization, is assessed in Fig. 9, with Fig. 9a showing the spatial distribution of mesh quality and Fig. 9b presenting the quality distribution histogram, mirroring the style of the forward mesh quality analysis in Fig. 2. This consistency validates the coupled hydro-geophysical approach, reinforcing

the model's ability to detect copper-rich zones through integrated hydrological and geophysical signatures, despite challenges in resolving fine-scale variations.

The impact of mesh resolution on solution accuracy was addressed by refining the forward mesh to a minimum cell size of approximately 0.146 m, particularly around the mineralized zone, where sharp gradients in ion concentration and velocity are expected. This refinement, combined with adjusted hydraulic conductivity values to a maximum of 2.12×10^{-5} m/s, reduced the CFL number to approximately 0.063, ensuring numerical stability in the advection-diffusion simulation. The enhanced mesh resolution, as shown in the forward mesh quality assessment (Fig. 2), improved the accuracy of ion transport calculations by better resolving spatial variations in the velocity field and concentration gradients. This also supported the reliability of subsequent ERT results by providing a stable foundation for forward modeling, addressing concerns about potential numerical errors arising from coarse mesh resolution.

To evaluate the inversion process, Table 3 presents the number of iterations and χ_N^2 values for each of the four time frames, providing insight into the convergence and goodness of fit of the inverted electrical resistivity models. χ_N^2 values near 1 indicate an optimal balance between data fit and model complexity, enhancing confidence in detecting the mineralized zone. Additionally, Table 4 summarizes the mesh characteristics, detailing the forward mesh (7981 triangular cells, 4102 nodes) and inversion mesh (2214 triangular cells, 1193 nodes), confirming sufficient resolution for accurate simulation and inversion. The results collectively demonstrate the model's capacity to simulate coupled hydro-geophysical processes, with velocity patterns informing ion transport and the inversion of synthetic ERT datasets providing a geophysical signature. The mineralized zone's influence on flow and resistivity underscores its detectability, though challenges persist in resolving fine-scale heterogeneity, aligning with advanced hydro-geophysical techniques and suggesting potential for refining exploration strategies in porphyry copper systems.

Table 3. Post-inversion parameters to evaluate inversion accuracy.

Time Frame - Inversion	Number of Iterations	χ_N^2	Time to Run (s)
1	3	0.5	56.29
2	4	0.27	68.16
3	6	0.92	104.13
4	13	0.73	241.30

Table 4. Meshing Parameters.

Mesh Type	Cell type	Cell Count	Node Count
Forward Mesh	Triangular	7981	4102
Inversion Mesh	Triangular	2214	1193

5 Conclusion

This study has effectively developed a coupled hydro-geophysical finite-element model to simulate subsurface flow, ion diffusion, and time-lapse ERT within a 2D representation of a porphyry copper deposit, offering a non-invasive exploration strategy. Utilizing the pyGIMLi framework, the model seamlessly integrates layered geological units, including an aquifer, host rock, basement, and mineralized zone,

accurately reflecting the interaction between hydraulic and electrical properties. The simulations demonstrated groundwater-driven ion transport, with dispersivity influencing concentration distributions, while time-lapse ERT, enhanced by inversion with the CGLS algorithm, successfully identified resistivity anomalies linked to the mineralized zone. Validation against velocity gradients from forward modeling confirmed the reliability of the inverted electrical resistivity profiles, with mesh quality assessments further supporting the model's precision in capturing subsurface heterogeneity.

The synergy of hydrological and geophysical datasets, bolstered by CGLS inversion, provides a powerful tool for investigating intricate porphyry copper systems. The resulting 2D resistivity models and mesh quality evaluations highlight the approach's accuracy, though limitations in resolving fine-scale geological variations remain. Detailed codes and computational implementations are presented in Appendix A, facilitating reproducibility and application by other researchers. Future research could extend the model to three dimensions or incorporate advanced inversion methods to enhance resolution, while field-based validation would improve its practical utility. This adaptable framework advances sustainable mineral exploration, marking a significant step forward in the development of integrated hydro-geophysical techniques.

References

Batayneh, A. T., and Al-Diabat, A. A., 2002, Akingboye, A. S., & Ogunyele, A. C. (2019). Insight into seismic refraction and electrical resistivity tomography techniques in subsurface investigations. Rudarsko Geolosko Naftni Zbornik, 34(1), 93–111. https://doi.org/10.17794/rgn.2019.1.9

Berger, B. R., Ayuso, R. A., Wynn, J. C., & Seal, R. R. (2008). Preliminary model of porphyry copper deposits. https://doi.org/10.3133/ofr20081321

Binley, A. (2015a). Tools and Techniques: Electrical Methods. Treatise on Geophysics: Second Edition, 11, 233–259. https://doi.org/10.1016/B978-0-444-53802-4.00192-5

Binley, A. (2015b). Tools and Techniques: Electrical Methods. In Treatise on Geophysics (pp. 233–259). Elsevier. https://doi.org/10.1016/B978-0-444-53802-4.00192-5

Christensen, N. K., Christensen, S., & Ferre, T. P. A. (2016). Testing alternative uses of electromagnetic data to reduce the prediction error of groundwater models. Hydrology and Earth System Sciences, 20(5), 1925–1946. https://doi.org/10.5194/hess-20-1925-2016

Field, D. A. (2000). Qualitative measures for initial meshes. International Journal for Numerical Methods in Engineering, 47(4), 887–906. https://doi.org/10.1002/(SICI)1097-0207(20000210)47:4<887::AID-NME804>3.0.CO;2-H

González-Quirós, A., & Comte, J.-C. (2021). Hydro-geophysical model calibration and uncertainty analysis via full integration of PEST/PEST++ and COMSOL. Environmental Modelling & Software, 145, 105183. https://doi.org/10.1016/j.envsoft.2021.105183

Hinnell, A. C., Ferré, T. P. A., Vrugt, J. A., Huisman, J. A., Moysey, S., Rings, J., & Kowalsky, M. B. (2010). Improved extraction of hydrologic information from geophysical data through coupled hydro-geophysical inversion. Water Resources Research, 46(4). https://doi.org/10.1029/2008WR007060

Johnson, T. C., Versteeg, R. J., Ward, A., Day-Lewis, F. D., & Revil, A. (2010). Improved hydro-geophysical characterization and

monitoring through parallel modeling and inversion of time-domain resistivity andinduced-polarization data. GEOPHYSICS, 75(4), WA27–WA41. https://doi.org/10.1190/1.3475513

Lesmes, D. P., & Friedman, S. P. (2005). Relationships between the Electrical and Hydrogeological Properties of Rocks and Soils (pp. 87–128). https://doi.org/10.1007/1-4020-3102-5_4

Linde, N. (2014). Falsification and corroboration of conceptual hydrological models using geophysical data. WIREs Water, 1(2), 151–171. https://doi.org/10.1002/wat2.1011

Linde, N., Renard, P., Mukerji, T., & Caers, J. (2015). Geological realism in hydrogeological and geophysical inverse modeling: A review. Advances in Water Resources, 86, 86–101. https://doi.org/10.1016/j.advwatres.2015.09.019

Lovell, M. A., & Pezard, P. A. (1990). Electrical properties of basalts from DSDP Hole 504B: a key to the evaluation of pore space morphology. Geological Society, London, Special Publications, 48(1), 339–345. https://doi.org/10.1144/GSL.SP.1990.048.01.28

Lu, B., Zhang, X., & Dai, Z. (2024). A CGLS-based method for solving magnetic moments of hybrid-model magnetic targets. Measurement Science and Technology, 35(7), 076119. https://doi.org/10.1088/1361-6501/ad3c5c

Mazáč, O., Kelly, W. E., & Landa, I. (1985). A hydro-geophysical model for relations between electrical and hydraulic properties of aquifers. Journal of Hydrology, 79(1–2), 1–19. https://doi.org/10.1016/0022-1694(85)90178-7

Moysey, S. (2007). Hydrogeophysics. Groundwater, 45(1), 8–8. https://doi.org/10.1111/j.1745-6584.2006.00286.x

Notario del Pino, J., & Díaz, R. (1998). Pesticide distribution and movement. Biotherapy, 11(2/3), 69–76. https://doi.org/10.1023/A:1007961524517

Nwankwoala, H., & Udom, G. (2009). Hydrogeophysics: An overview of general concepts, applications and future perspectives. Scientia Africana, 7(2). https://doi.org/10.4314/sa.v7i2.46018

Østerby, O. (2002). Five Ways of Reducing the Crank-Nicolson Oscillations. DAIMI Report Series, 31(558). https://doi.org/10.7146/dpb.v31i558.7115

Portniaguine, O., & Zhdanov, M. S. (1999). Focusing geophysical inversion images. In GEOPHYSICS (Vol. 64, Issue 3). http://library.seg.org/

Rücker, C., Günther, T., & Wagner, F. M. (2017). pyGIMLi: An open-source library for modelling and inversion in geophysics. Computers and Geosciences, 109, 106–123. https://doi.org/10.1016/j.cageo.2017.07.011

Warburton, T., & Hagstrom, T. (2008). Taming the CFL Number for Discontinuous Galerkin Methods on Structured Meshes. SIAM Journal on Numerical Analysis, 46(6), 3151–3180. https://doi.org/10.1137/060672601

Yazdanpanah, A., & Abedi, M. (2024). Geophysical simulation of landslide model based on electrical resistivity and refraction seismic tomography through unstructured meshing. International Journal of Mining and Geo-Engineering, 58(3), 263–270. https://doi.org/10.22059/ijmge.2024.370406.59.